Applied Physics B (2021) 127:43
https://doi.org/10.1007/s00340-021-07590-0

Applied Physics B
Lasers and Optics

Thermal and optical performance of cryogenically cooled laser diode bars mounted on pin-finned microcoolers

K. J. Kim[1] · B. Han[2] · A. Bar-Cohen[2]

Received: 26 January 2020 / Accepted: 8 February 2021 / Published online: 28 February 2021

Abstract
This study investigates the thermal performance of cryogenic micro-pin fin coolers for high-power laser diode (LD) bars. An open-loop liquid nitrogen cooling system, used to operate LD bars at cryogenic temperatures, is developed and characterized. The comparison study demonstrates that the total thermal resistance value of the micro-pin fin cooler, ranging from 0.03 to 0.04 °C/W, is only 1/3 of that of the micro-gap cooler and, thus, contributes significantly to reducing the LD operating temperature and enhancing its efficiency. In this study, the peak optical power of 68.8 W was observed at an LD bar package base temperature of − 100 °C, providing a 20% increase relative to the optical power of 57.3 W for a nominal operating condition with an LD bar package base temperature of 41 °C. This result clearly illustrates the enhancement in optical performance made possible by cryogenic cooling with a pin fin microcooler.

1 Introduction

Growing interest in high-power laser diodes for applications in defense, metal cutting and processing technologies, medical treatments, and communication applications [1, 2] has placed new demands on the output power and efficiency of laser diode (LD) light sources, most notably LD bars containing multiple emitters [1]. A nominal heat "density"—or heat flux—of the high-power LD bar is a formidable 50 W/cm^2, necessitating aggressive thermal management to avoid deterioration of the optical performance of such LD bars at elevated temperatures. Zhang et al. [2] demonstrated the strong coupling of the power distribution of high-power LD arrays with junction temperature. Kim et al. [1] observed that junction temperature variations of high-power LD arrays induce asymmetry in the power spectrum and lead to spectral broadening. It is, thus, essential that advanced thermal management techniques be applied to single bars, packages, and modules of high-performance LDs.

The use of two-phase liquid cooling [3–11] in the microcoolers supporting the LD bars might alleviate some or all of the thermally driven adverse effects on optical performances of high-power lasers. Rigorous research activities [4–8] have been recently reported on such two-phase flows in micro- or mini-pin fin arrays, as would be used inside the liquid microcoolers. Resser et al. [4] investigated 305 µm high staggered and in-line square pin fin arrays with deionized water and HFE-7200. The average base area heat transfer coefficients were about 30 kW/m^2-K with deionized water and 7 kW/m^2-K with HFE-7200. The average pressure drops were about 35 kPa with deionized water and 30 kPa with HFE-7200. David et al. [5] studied 1000 µm high, staggered, square pin fin arrays with R-134a, and the average base area heat transfer coefficient was about 25 kW/m^2-K. McNeil et al. [6] explored 1000 µm high, in-line, square pin fin arrays with R-113. The average heat transfer coefficient was about 3.5 kW/m^2-K, and the average pressure drop was about 3 kPa. Qu et al. [7] investigated 670 µm high staggered square pin fin arrays with water and the average heat transfer coefficient was about 70 kW/m^2-K. Krishnamurthy et al. [8] studied 200 µm high staggered circular pin fin arrays with water, and achieved an average heat transfer coefficient of approximately 60 kW/m^2-K.

Refrigeration cooling is another potentially effective solution for high-power LD bars, operating with extreme heat

✉ B. Han
bthan@umd.edu

✉ A. Bar-Cohen
Avi.Bar.Cohen@Raytheon.com

K. J. Kim
kjkim@pknu.ac.kr

[1] Mechanical Design Engineering, Pukyong National University, Busan, Korea

[2] Mechanical Engineering, University of Maryland, College Park, MD, USA

densities, due to the expected improvement of the optical performance at sub-ambient temperatures. Lowering the operating temperature of the LD bar can be expected to reduce the internal losses and raise both the quantum and wall plug efficiency by a considerable factor, estimated by some to fall in the range of 0.2–0.5%/K [12]. To the best of our knowledge, no research result has been reported regarding cryogenic evaporative cooling of LDs with a finned microcooler. Hence, this study aims to develop the instrumentation and perform an exploratory investigation of cryogenic cooling with micro-pin fin array to quantify the potential benefit of cryogenic evaporative thermal control of high-power LD bars.

This paper expands on an earlier presentation at the 2019 DE S and T Symposium [13] and begins by summarizing the results of a basic investigation of a micro-pin fin array with FC-72 as a working fluid. Then, the paper describes the design and fabrication of a test rig to enable the operation of cryogenic microcoolers with liquid nitrogen (LN_2) flows. Finally, the paper presents the thermal performance of a cryogenic micro-pin fin cooler and its application for cooling an actual LD bar.

2 LN_2-cooled micro-pin fin array

Table 1 compares properties of N_2 and FC-72 at a pressure of 1 atm. Table 1 shows that crucial thermofluid properties such as latent heat of vaporization and liquid specific heat for N_2 are about twice as large as those for FC-72. The table also reveals that the LN_2 thermal conductivity is 2.4 times larger and the kinematic viscosity just half of the respective values for FC-72. The table also indicates a 5 times smaller Prandtl number, Pr, and comparable Jacob number, Ja, of N_2 compared with those of FC-72. The comparison between N_2 and FC-72 properties suggests that N_2 would be better for heat transfer enhancement in both sensible and latent heat transfer modes.

Table 1 Properties of N_2 and FC-72 at a pressure of 1 atm [14–17]

Property	Units	N_2	FC-72
Molecular weight		28	338
Boiling temperature	K °C	77.3 − 195.9	329.1 56
Liquid enthalpy	kJ/kg	− 122.1	59.8
Latent heat of vaporization	kJ/kg	198.8	84.7
Vapor enthalpy	kJ/kg	76.7	144.5
Liquid density	kg/m^3	806	1680
Vapor density	kg/m^3	4.6	13
Kinematic viscosity of liquid	10^6 m^2/s	0.19	0.38
Liquid specific heat	kJ/kg-K	2.041	1.1
Liquid thermal conductivity	W/m-K	0.135	0.057
Thermal diffusivity	10^6 m^2/s	0.082	0.031

FC-72, a dielectric liquid, has been extensively used to explore two-phase heat transfer through small channels in microcoolers used for thermal management of electronic components. Hence, recognizing the differences between N_2 and FC-72 and the complexity of performing cryogenic experiments, a preliminary experimental study was conducted using FC-72 as the working fluid to investigate basic characteristics of the selected parameters for the micro-pin fin array that could be used to cryogenically cool an LD bar.

Figures 1a and b show the in-line copper micro-pin fin array selected for this study and the micro-pin fin array test section, respectively. The micro-pin fin array is embedded into the test section. Each pin fin is 150 µm wide and either 100 µm or 500 µm tall, with a pin-to-pin pitch of 300 µm. The footprint of the pin fin array is 12 mm × 12 mm, and the number of fins is 1600.

A ceramic resistive heater provides the lower surface of the pin fins with a uniform heat flux. Five embedded thermocouples, positioned along the centerline of the pin fin array, were used for temperature measurement. The PEEK manifold channels the fluid flow to and from the pin fins. The sapphire window enables top–down photographic and mid-wave infrared visualization.

The measured values were used to determine the base heat transfer coefficients, i.e., the average heat transfer coefficients for the base area of the pin fin array. The base heat transfer coefficient is defined as follows:

$$h_{base} = \frac{q}{A\left(T_s - T_\infty\right)}, \tag{1}$$

where q is a heat transfer rate, A is a base area, T_s is a surface area, and T_∞ is a fluid temperature.

Figure 2 shows the variation of the heat transfer coefficient as a function of mass vapor fraction, i.e., flow quality, for both the 100–500 µm tall pin fin arrays, with the symbols showing the measured data and the lines (dotted and solid), the predictions obtained from the Reeser et al. correlation for a similar array of pin fins [4]. Reeser et al. correlation was the only available correlation including the full range of exit qualities up to 90% for micro-pin fin arrays. The correlation was developed using deionized water and HFE-7200 as working fluids, and its prediction yielded 3% mean average error (MAE) for the water heat transfer coefficient and 10–13% MAE for the HFE-7200 heat transfer coefficient.

The results obtained from the 100 µm tall pin fin channel are shown at flow rates of 0.5, 0.75, and 1.0 mL/s, while the results of the 500 µm tall pin fin channel are shown at a flow rate of 1.0 mL/s. Exit flow qualities were

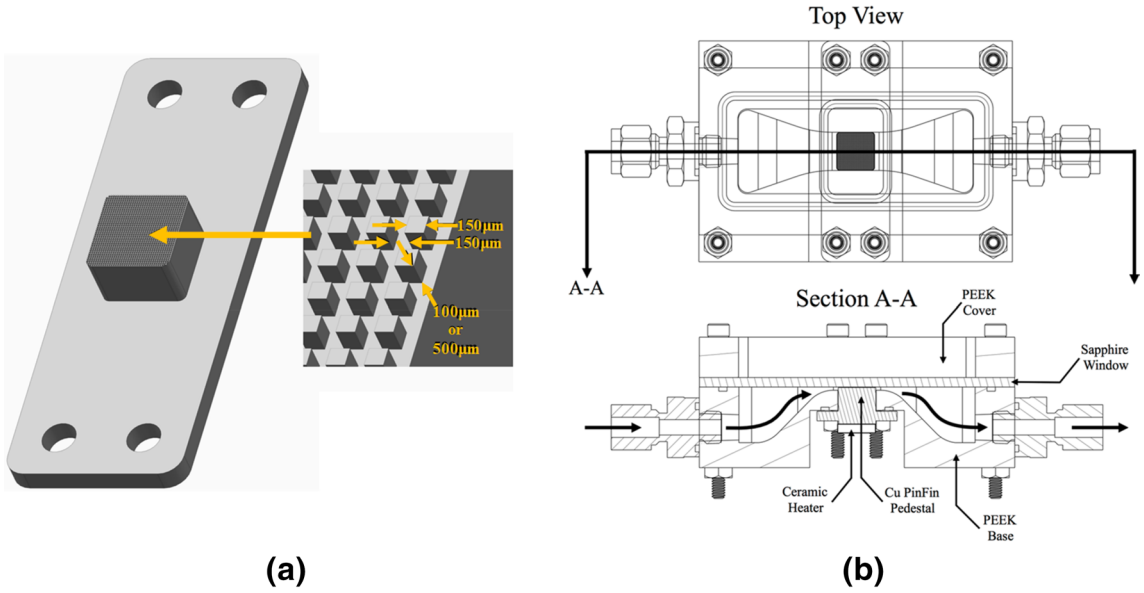

Fig. 1 **a** A copper micro-pin fin array and **b** the test section of the micro-pin fin array

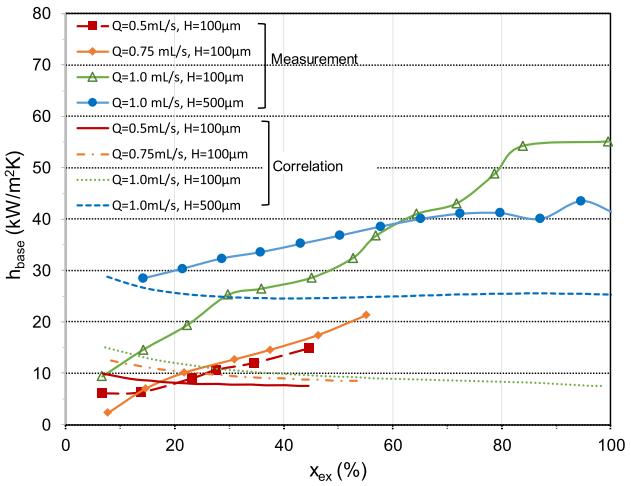

Fig. 2 Base heat transfer coefficients, h_{base}, as a function of exit quality, X_{ex}, for two-phase micro-pin fin channels

determined by considering measured flow rates, heater powers, and the value of latent heat of vaporization. The inlet flow qualities were assumed to be zero in the evaluation.

The experimental results show that the base heat transfer coefficient typically falls in the very high range of 10–40 kW/m^2-K, and generally enhances with an increase in the exit flow quality (or heat flux) until dryout (or thermal runaway) is reached. While for the 100 micron pin fins studied, increasing the flow rate from 0.5 to 0.75 mL/s led to a very modest increase in the heat transfer coefficient, a further increase to 1.0 mL/s resulted in nearly a doubling of the base area heat transfer coefficient and safe operation across the full range of qualities.

Interestingly, use of taller pin fins—shifting from 100 microns high to 500 microns high—at a flow rate of 1.0 mL/s resulted in a negligible increase in the average value of the base heat transfer coefficients for the whole quality range, but did provide higher values at the low qualities and lower heat transfer coefficient values at the high qualities.

It is seen that the Reeser et al. correlation [4] provides rough agreement with the measured heat transfer coefficient at intermediate qualities but while the measured results show a consistent enhancement of the base heat transfer coefficient with the increase of the exit quality until dry out is reached, the correlation displays a nearly flat, though slightly decreasing, trend.

An actual high-power LD bar typically consists of 10–40 emitters, with a center wavelength ranging from 800 to 1550 nm [18]. Power efficiency (conversion efficiency from electrical power to optical power) is about 60% for the optimum high-power LD bar at room temperature. It should be noted that a thermal power, also referred to as a power dissipation, is a dissipated heat flow rate. Considering a brief energy balance around the LD bar, the thermal power can be evaluated. For example, assume that the electrical power input to the LD bar is 100 W, and the power efficiency of the LD bar is 60%. Then, the optical power is 60 W and thermal power is 40 W.

For the nominal heat density of LD bars of 50 W/cm^2, if a heat transfer coefficient of 20 kW/m^2-K could be obtained with LN_2—equal to the typical heat transfer coefficients with FC-72 shown in Fig. 2—the temperature rise of the LD bar

above the saturation temperature of the LN_2 would be just 25 K, assuring high-power cryogenic operation of the laser diodes at a temperature of approximately 102 K (− 171 °C). Hence, the micro-pin fin array should be tested at cryogenic temperatures.

3 Apparatus of cryogenic micro-pin fin coolers

This section discusses the structure of the micro-pin fin cooler and the LN_2 flow apparatus to test the micro-pin fin cooler. A cross-sectional and exploded view of the cryogenic micro-pin fin cooler is presented in Fig. 3. Figure 4a –to c shows an assembled LN_2 apparatus, the schematic of a LN_2 flow loop, and the thermocouple locations on the micro-pin fin cooler manifold.

In this study, the performance of an un-finned, micro-gap cooler was also explored, and it served as the baseline of the analysis. The micro-gap cooler denotes a cooler containing a micro-gap [3] without a micro-pin fin array. Its structure is very similar to the micro-pin fin cooler shown in Fig. 3 except for the "open" micro-gap instead of a channel populated with micro-pin fins. It should be also noted that the metrology and operating conditions, as shown in Fig. 4, for both the micro-pin fin and gap coolers are very similar.

In Fig. 3, the working fluid is LN_2 for the cooler. A central manifold, an upper insert, and a lower insert compose the cooler, and the base material for the parts is copper. The central manifold dimension is 55.1 mm × 24.9 mm x 30 mm. Building on the available results and striving for high base heat transfer coefficients at modest pressure drops, each pin fin is 150 µm wide and 300 µm tall. The pin pitch for both stream-wise and transverse directions is 300 µm. References [4] to [8] show the width of the micro-pin fin ranging from 100 µm to 350 µm and the pitch of the micro-pin fin array ranging from 150 µm to 431 µm. To select 150 µm fin width and 300 µm pitch, the values of the references and the fabrication capability were also considered. The footprint of the array is 10 mm × 10 mm. As shown in Fig. 3, three parts of the cooler are bolted together. Contact surfaces are sealed using a flexible cryogenic sealant.

The initial challenges of the test loop—ice generation on the LD emitter surface and system startup time reduction—were resolved by an aerogel insulation layer and nitrogen shield gas. The LN_2 tank's integrated pressure regulator controls the flow of LN_2. The temperature (T_{INLET}) and the pressure (P_{INLET}) are measured at the first four-way junction. The measurement locations are clearly shown in Fig. 4b. An Omega E-Type thermocouple and a cryogenic pressure transducer are used for the measurement. The LN_2 flow absorbs the heat from the LD bar, and the phase change occurs from liquid to vapor at the LD microcooler. The temperature (T_{OUTLET}) and the pressure (P_{OUTLET}) of the saturated LN_2 flow are measured at the second four-way junction. The heat exchanger, shown in Figs. 4a and b, completely evaporates all of the excess LN_2 and heats the LN_2 using the water loop consistently maintained at 25 °C. After the heat exchanger, the temperature of the nitrogen gas is monitored to confirm the evaporation and heating of the LN_2.

All the compression fittings and tubing are made of 316SS, and the apparatus is insulated using Cryogel Z insulation. Data is acquired in LabVIEW using a NI 9214 temperature input module and NI 9205 voltage input module. Figure 4c shows thermocouple locations for the preliminary heater-based tests of the micro-pin fin cooler manifold prior to the actual test for the LD bar cooling.

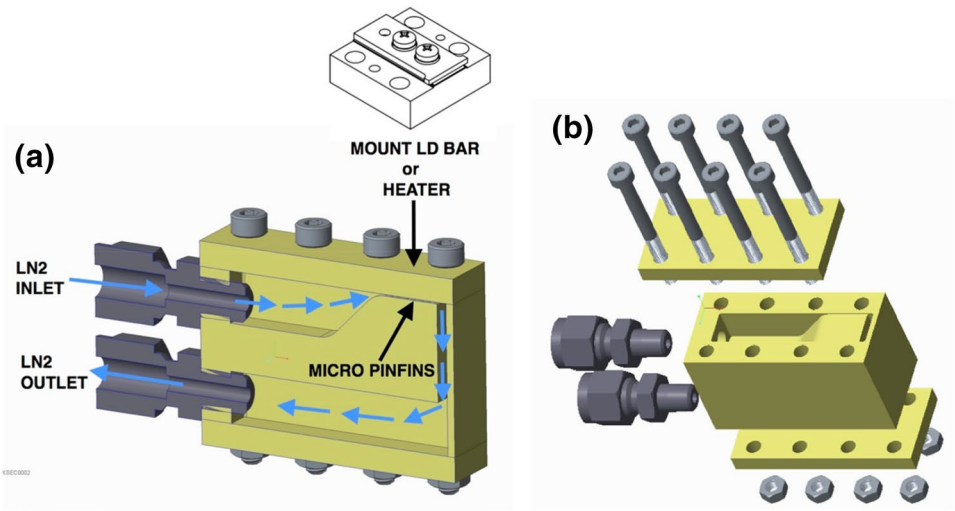

Fig. 3 Cross-sectional (**a**) and exploded view (**b**) of the cryogenic micro-pin fin cooler [3]

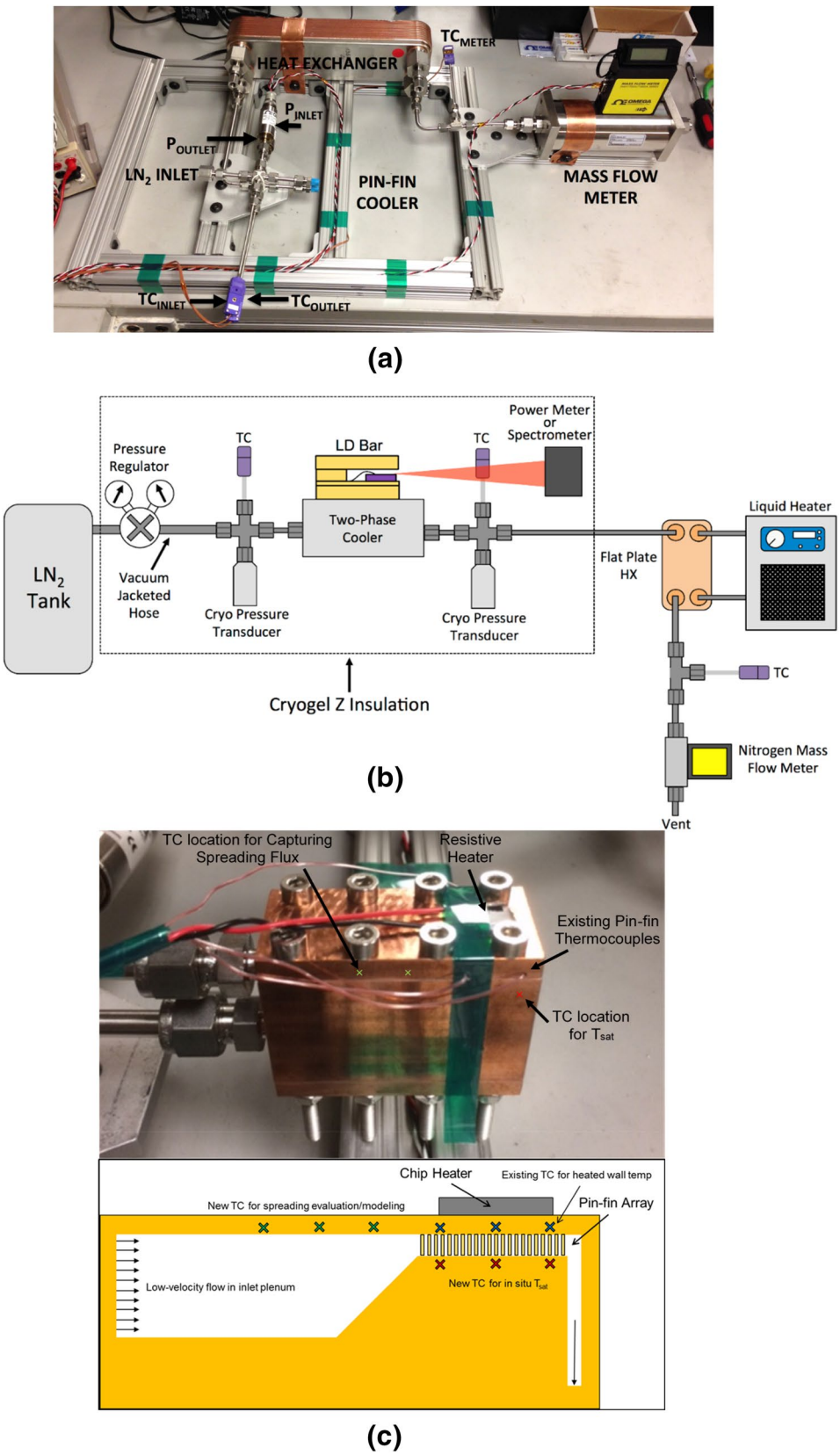

Fig. 4 **a** Assembled LN_2 flow loop apparatus, **b** a schematic of LN_2 flow loop apparatus, and **c** thermocouple locations on the micro-pin fin cooler manifold [3]

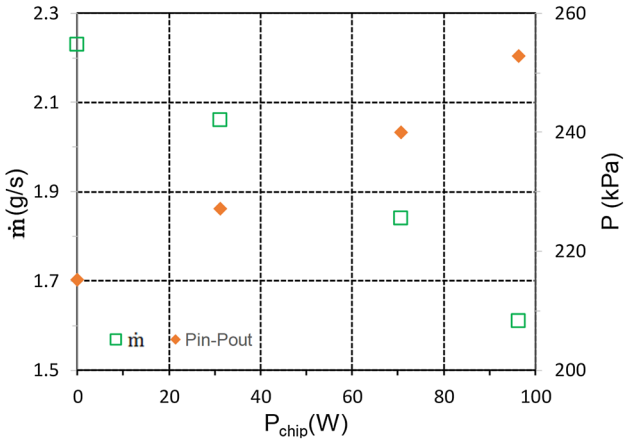

Fig. 5 Left axis: fluid mass flow rate, $\dot{m}$, as a function of applied chip heater power, P_{chip}. Right axis: pressure difference between inlet and outlet, $P_{in} - P_{out}$

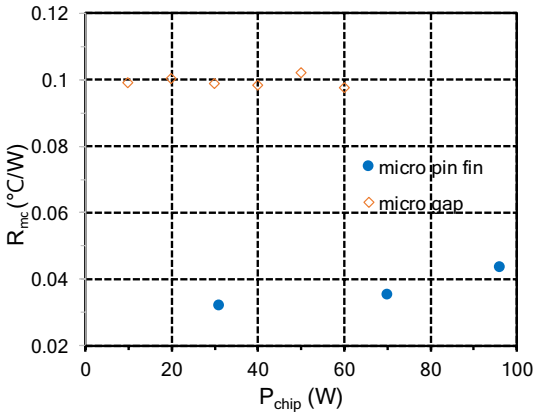

Fig. 6 Thermal resistance, R_{mc}, of the micro-pin fin cooler and the micro-gap cooler as a function of applied chip heater power, P_{chip}

4 Thermofluid performance of cryogenic micro-pin fin coolers

4.1 Flow performances

The thermofluid performance of a cryogenic pin fin microcooler was explored utilizing the test rig presented in Fig. 4. The primary findings of the investigation are summarized in Figs. 5 and 6. It is to be noted that the micro-pin fin height is 300 µm and the micro-gap is 330 µm.

Heat dissipated from the chip increases the vapor fraction, or quality, of the flowing LN_2 and requires an ever greater pressure difference to drive higher quality vapor/liquid mixture through the pin-finned microchannels. Since the pressure driving the flow of LN_2, in this "blow-down" experiment, is fixed at 370 kPa and the ambient pressure is fixed at atmospheric pressure, increasing power dissipation results in a reduced mass flow rate through the microchannels, as clearly seen in Fig. 5.

It is to be noted that the increasing momentum dissipation, associated with higher vapor fraction flow and leading to reduced mass flow in the microchannels, could spiral out of control and result in a "runaway" condition—producing vanishingly low flow rates and spiking wall temperatures. Such conditions were observed in this study at chip power dissipation of 126 W. Unpowering the chip heater, at this point, allowed a slow recovery of the liquid flow in a matter of minutes, due to sufficient thermal mass in the manifold to prevent a catastrophic temperature rise. The observed "runaway" power dissipation of 126 W was approximately twice the expected power dissipation of this commercial LD bar, and did not interfere with completion of this study. Moreover, in a more sophisticated experiment or actual application, an automated flow control method could be used to prevent this flow instability.

A pressure drop represents the quantitative effect of a flow resistance. In this study, the pressure drops both in a subcooled regime and a saturated regime should be considered. Principle parameters affecting the pressure drop are viscosity, density, local quality, fluid velocity, and characteristic length. The pressure drop correlation and such parameters are found in the reference [4]. The considerable difference of the pressure drops between two regimes, interrelated fluid properties, flow conditions, and geometric characteristics of the micro-pin fin cooler result in very complicated pressure drop mechanism. Hence, the prediction of the pressure drop behavior for LN_2 or FC-72 through the micro-pin fin cooler would be quite challenging.

Nevertheless, the pressure drop correlation [4] may suggest the following rough prediction. In a low-quality regime, the pressure drop with FC-72 might be greater than that with LN_2 while in a high-quality regime, the pressure drop with FC-72 would be comparable to the LN_2 case. Apparently, the higher pressure drop is, the more attendant power requirement is. It should be noted that typical operating temperatures of high-power LDs range from 20 °C to 30 °C [18]. The boiling temperature of FC-72 is 56 °C shown in Table. 1. Hence, FC-72 may not be appropriate to cool high-power LDs despite its promising potentials for cooling high-power electronics.

4.2 Thermal performances

4.2.1 Definitions of thermal resistance

The overall thermal resistance, R_T, of an electronic system, defined as follows:

$$R_T = \Delta T / q_{diss}, \tag{2}$$

where ΔT is the temperature difference between a heat source, i.e., a junction, and a coolant, and q_{diss} is the dissipated heat. These terms are used for a common Figure-of-Merit for thermal management of solid-state systems.

The LD bar thermal resistance, R_{jc} is defined as follows:

$$R_{jc} = \left(T_j - T_{case}\right)/q_{diss}, \tag{3}$$

where T_j is the diode junction temperature, and T_{case} is the case temperature of the LD bar.

For an actual LD bar, R_T includes the R_{jc} of the LD bar, the conduction resistance, and a combination of the single-phase convection resistance, near the inlet, and the two-phase convection resistance in the majority of the wetted area of the microcooler. The conduction resistance includes the spreading resistance between the LD bar and the microcooler, the contact resistance at the interface between the LD bar and the microcooler, and the conduction resistance through the wall thickness of the microcooler.

Hence, R_T can be redefined as follows:

$$R_T = R_{jc} + R_{mc} + R_{sp} + R_{cont}, \tag{4}$$

where R_{mc} is the thermal resistance of the microcooler, R_{sp} is the spreading resistance, and R_{cont} is the contact resistance.

The preliminary test results of the micro-pin fin array with FC-72, yielding an overall resistance of 0.23 °C/W, and consideration of the expected FC-72 heat transfer coefficients [4], suggest that the conduction terms would dominate R_T. The effective thermal resistance from the junction to the case of the commercial LD bar, employed in this study, is 0.8 °C/W [3]. It should be noted that the chip heater (Fig. 4c), simulating heat dissipation of the LD bar, was used to measure R_{mc} values of the micro-pin fin cooler and the micro-gap cooler.

Figure 6 shows the thermal resistance, R_{mc}, of the micro-pin fin cooler and the "baseline" micro-gap cooler, both with a LN_2 flow. The R_{mc} values for the micro-pin fin cooler, increasing with the increase of the power dissipation, range from 0.03 to 0.04 °C/W, while those for the micro-gap cooler are almost constant at 0.1 °C/W. The R_{mc} values of the micro-pin fin cooler are, thus, nearly 3 times lower than those of the micro-gap cooler. Such superiority in thermal resistance, which results in just a 1 °C rise at 30 W and 3 °C temperature rise at 100 W of dissipation, can be ascribed primarily to the 2.75 times surface area enhancement by the pin fin array. The observed increase in the pin-finned microcooler resistance, R_{mc}, with the increase of the power dissipation, as is clearly displayed in Fig. 5, is thought to reflect the impact of the previously discussed drop-off in the LN_2 flow rate as the power dissipation and vapor fraction increase.

In Fig. 6, for the micro-pin fin cooler, LN_2 mass flow rates are 2.06 g/s at 30 W, 1.84 g/s at 70 W, and 1.61 g/s at 96 W. These mass flow rate values are clearly shown in Fig. 5. For the micro-gap cooler, the LN_2 mass flow rate is 2.3 g/s for the chip heater powers ranging from 10 to 60 W shown in Fig. 6. All the data presented in Figs. 5 and 6 were generated employing the setup shown in Fig. 4c. It should be noted that a resistive heater was used for the test. Thus, the interface temperature defined for the LD bar package, shown in Fig. 7, cannot be determined for the results in Figs. 5 and 6. Nevertheless, the resistive heater could be considered as an isothermal body.

5 Application of cryogenic micro-pin fin coolers for high-power LD bars

The performance of the cryogenic micro-pin fin cooler for an actual high-power LD bar is evaluated and discussed in this section. The LD bar used for the investigation is a DILAS conduction cooled LD bar consisting of 19 GaAs emitters [18]. The length of the bar is 2 mm. The maximum optical power is 65 W at 62.5 A with a center wavelength of 976 nm ± 10 nm, and the overall efficiency at 25 °C is 63.4%. Figure 7 shows a schematic view of the LD bar package and the actual test rig containing the LD bar package mounted on the micro-pin fin cooler with the nitrogen flow loop.

Results from the performance test are summarized in Fig. 8a and b, presenting the optical power emitted by the LD bar, the emitter temperatures of the LD bar, and the power efficiency of the LD bar as a function of interface temperature between the LD bar package and the upper surface of the cryogenic micro-pin fin cooler. It should be noted that the LD bar package runs at 60 A emitter current in the measurement. The emitter temperature was determined by considering heat dissipations and the thermal resistance from the emitter to the heat spreader of the LD bar. Heat dissipation was evaluated by subtracting the emitted optical power from the electrical power input to the LD bar. The emitter temperature was determined using the following equation:

$$T_e = T_i + q \times R_{jc}, \tag{5}$$

where T_e is the emitter temperature, T_i is the interface temperature, q is the heat dissipation, and R_{jc} is the thermal resistance of the LD bar, i.e., the thermal resistance from the emitter to the LD bar heat spreader. The R_{jc} used for the measurement is 0.8 °C/W.

Figure 8 reveals a bifurcated performance curve for the cryogenically cooled LD bar, with optical power and efficiency increasing moderately as the interface temperature decreases from 50 °C to – 100 °C, but then decreasing steeply

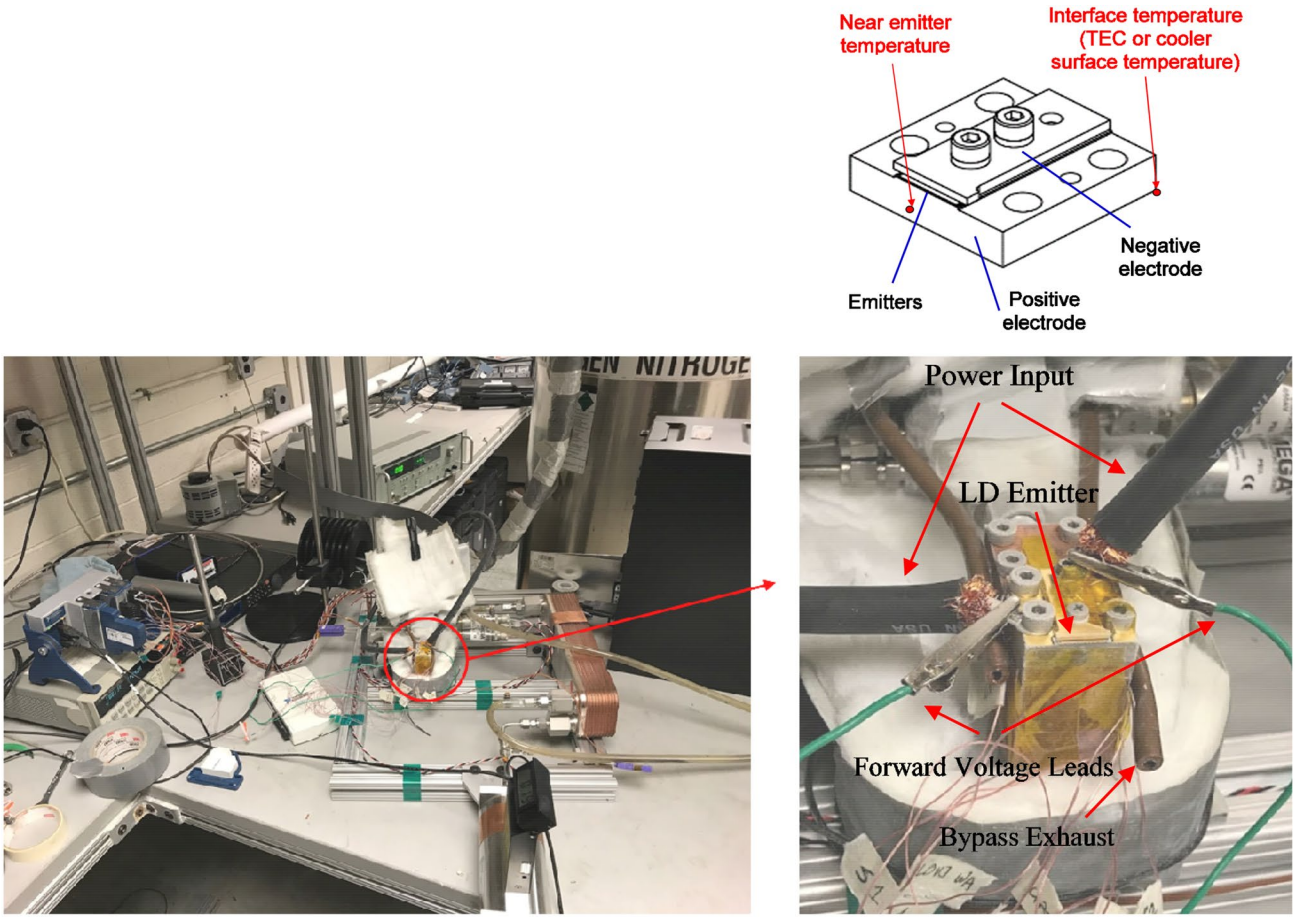

Fig. 7 A high-power LD bar package mounted on the micro-pin fin cooler with a nitrogen flow loop

as the temperature continues to fall towards − 200 °C. The peak optical power of this DILAS LD bar was, thus, found to occur at 68.8 W for an interface temperature of − 100 °C and an emitter temperature of − 75 °C.

It is, thus, clear that use of the cryogenic micro-pin fin cooler has considerably improved the optical performance of the LD bar, raising the peak power by some 20%, to nearly 69 W at an interface temperature of – 100 °C, compared with the nominal optical power of just 57.3 W at an interface temperature of 41 °C. The peak power efficiency of 68.9%—some 5% higher than for room temperature operation—is seen to occur at an interface temperature of – 50 °C, remains essentially flat from – 50 °C to – 100 °C and then falls steeply below − 100 °C.

The observed deterioration of performance below − 100 °C was unexpected and will require additional research to determine the underlying causes and mechanisms responsible for this result. Despite the use of a nitrogen gas shield, ice film generation on the emitter surface was observed in the actual test, for interface temperatures of − 100 °C and colder. This ice accumulation may well explain the observed degradation in the optical power and the power efficiency below − 100 °C. Alternatively, the complex—and sometimes competing ways—in which the emitter temperature can affect the threshold current, the external differential quantum efficiency, and the power efficiency, as well as how they interact to determine the emitted optical power [19] may be responsible for the observed behavior of this commercial cryogenically cooled GaAs LD bar.

The goal of this study is not to demonstrate the improved performance of the typical high-power LD under absolutely cryogenic temperatures in the range from − 196 °C to − 173 °C. The typical high-power LDs, commercially available, nominally operate around the room temperature. The primary objectives of this study are to explore the thermofluid performance of micro-pin fin coolers with LN_2 flow and to investigate the performance of the typical high-power LD in the broad range of temperatures from the near room temperature to the absolutely cryogenic temperature. For the absolute cryogenic temperature condition in the range from − 196 °C to − 173 °C, the LD with specially designed band structure might be needed. Nevertheless, as aforementioned, it is clearly seen that both the optical power and the power efficiency of the typical high-power LD could be

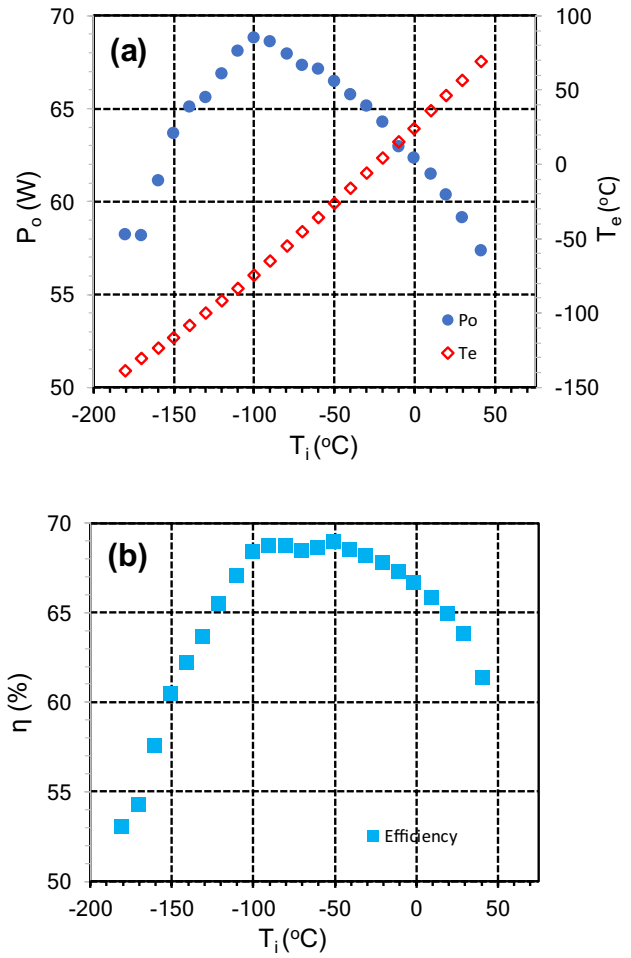

Fig. 8 **a** Optical powers, P_o, emitter temperatures, T_e, **b** power efficiency, η, of the high-power LD bar as a function of interface temperature, T_i

considerably improved in the range from the room temperature to – 100 °C.

6 Conclusions

This study was conducted to explore the thermal performances of cryogenic micro-pin fin coolers for high-power LD bars. The preliminary study explored the basic thermal behaviors of the micro-pin fin arrays with FC-72 as a working fluid. After the preliminary study, the apparatus was modified and implemented for exploring the performance of cryogenic micro-pin fin coolers with liquid nitrogen, LN_2, flows. The study analyzed the thermal performance of the cryogenic micro-pin fin cooler and demonstrated its application for cooling an actual LD bar.

The thermal resistance value for the micro-pin fin cooler, R_{mc}, from the hot surface of the cooler to the LN_2 flow, ranged from 0.03 to 0.04 °C/W. This value was just 1/3 of the resistance associated with the micro-gap cooler. Use of the cryogenic micro-pin fin cooler was found to considerably improve the optical performance of the LD bar, raising the peak power by some 20%, to nearly 69 W at an interface temperature of – 100 °C, compared with the nominal optical power of just 57.3 W at an interface temperature of 41 °C. Similarly, the peak power efficiency was found to reach 68.9%, or approximately 8% higher than achieved with a base temperature of 41 °C, was observed to occur at an interface temperature of – 50 °C.

Acknowledgements This material is based on research sponsored by Air Force Research Laboratory (AFRL) and the Defense Advanced Research Agency (DARPA) under agreement number FA8650-15-1-7526. The U.S. Government is authorized to reproduce and distribute reprints for Governmental purposes not withstanding any copyright notation thereon. The views and conclusions contained herein are those of the authors and should not be interpreted as necessarily representing the official policies or endorsements, either expressed or implied, of Air Force Research Laboratory (AFRL) and the Defense Advanced Research Agency (DARPA) or the U.S. Government.

References

1. D.-S. Kim, C. Holloway, B. Han, A. Bar-Cohen, Appl. Opt. **55**, 7487–7496 (2016)
2. P. Zhang, D.-S. Kim, B. Han, Appl. Opt. **56**, 5590–5598 (2017)
3. D.-S. Kim, M. Fish, B. Han, A. Bar-Cohen, DARPA Report, Contract No. FA8650-15-1-7526 (2017)
4. A. Reeser, A. Bar-Cohen, G. Hetsroni, Int. J. Heat. Mass. Tran. **78**, 974–985 (2014)
5. T. David, D. Mendler, A. Mosyak, A. Bar-Cohen, G. Hetsroni, J. Electron. Packag. **136**(021003), 1–10 (2014)
6. D.A. McNeil, A.H. Raeisi, P.A. Kew, P.R. Bobbili, Appl. Therm. Eng. **30**, 2412–2425 (2010)
7. W. Qu, A. Siu-Ho, Int. J. Heat. Mass. Tran. **52**, 1853–1863 (2009)
8. S. Krishnamurthy, Y. Peles, Int. J. Heat. Mass. Tran. **51**, 1349–1364 (2008)
9. E. Rahim, A. Bar-Cohen, Heat. Transfer. Eng. **36**, 511–520 (2015)
10. A. Bar-Cohen, C. Holloway, Interfacial. Phenom. Heat Transf. **3**, 393–412 (2016)
11. S.L. Qi, P. Zhang, R.Z. Wang, L.X. Xu, Int. J. Heat. Mass. Tran. **50**, 5017–5030 (2007)
12. M. Azawe, Int. J. Phys. Sci. **8**, 362–370 (2013)
13. K.J. Kim, M. Fish, A. Bar-Cohen, B. Han, DE S and T Symposium (2019)
14. B.A. Hands (ed.), *Cryogenic Engineering (Academic Press* (Niwot, CO, USA, 1986)
15. W.M. Haynes (ed.), *CRC Chemistry/Physics Handbook*, 93rd edn. (CRC press, New York, USA, 2013)
16. 3M Fluorinert Product Information (2000)
17. I. Mudawar, T.M. Anderson, J. Electron. Packag. **112**, 375–382 (1990)
18. DILAS Product Information, http://www.dilas.com/products/ (2020)
19. P. Crump, M. Grimshaw, J. Wang, W. Dong, S. Zhang, S. Das, J. Farmer, M. DeVito, L.S. Meng, J.K. Brasseur, OSA/QELS, Long Beach, California, U.S.A., JWB24 (2006)